Raman spectra of vanadates MV2O6 (M= Mn, Co, Ni, Zn) crystallized in the non-usual columbite-type structure

J.P. P Pena, Pierre Bouvier, M. Hneda, C. Goujon, O. Isnard

Raman spectra of vanadates $M\mathrm{V_2O_6}$ (M = Mn, Co, Ni, Zn) crystallized in the non-usual columbite-type structure

J. P. Peña[a,b], P. Bouvier[a], M. Hneda[c], C. Goujon[a], O. Isnard[a]

[a] *Université Grenoble Alpes, CNRS, Institut Néel, 25 rue des Martyrs, 38042, BP166X, Grenoble, France*
[b] *Universidade Federal do Rio Grande do Sul, Instituto de Física, Av Bento Gonçalves 9500, 91501-970 Porto Alegre*
[c] *Universidade Federal dos Vales do Jequitinhonha e Mucuri, Instituto de Engenharia, Ciência e Tecnologia, 39447-790, Janaúba, Brazil*

Abstract

We report the first Raman spectra for the vanadates with chemical formula $M\mathrm{V_2O_6}$ (M =Mn, Co, Ni, Zn) crystallized in a columbite-type structure (*Pbcn* space group). The columbite-type structure, which is quite unusual for the compounds $M\mathrm{V_2O_6}$, was obtained by synthesis at high temperature and pressure from precursor powder samples in either $P\overline{1}$ or *C2/m* structures. The cell parameters, interatomic distances, and distortion indexes of the octahedra in the *Pbcn* structure, were obtained from the Rietveld refinement of powder X-ray diffraction patterns measured at room temperature for each sample. The Raman modes were obtained from high quality spectra recorded in the range of wavenumbers between 50 and 1170 $\mathrm{cm^{-1}}$; these were assigned by comparison with the known spectra of the isostructural niobates $M\mathrm{Nb_2O_6}$. Common sequences of peaks can be identified in the Raman spectra of all the studied samples, but the position of those peaks in wavenumber $\bar{\omega}$ does not follow the behavior that is expected from looking only at the interatomic distances between the atoms involved in the vibration. The influence of the electronegativity of the atoms M in the force constants of the V-O bonds is proven in the evolution of the A_g Raman mode observed at the highest wavenumber.

Email address: jully.pena-pacheco@neel.cnrs.fr (J. P. Peña)

Keywords: oxide-vanadates, Raman spectroscopy, unconventional structural phases, high-pressure high-temperature synthesis

1. Introduction

It is well known in condensed matter that changing the crystal structure of one compound can radically change its physical properties even though the stoichiometry remains the same. For this reason, in the search for new technological capabilities and physical phenomena, studying the polymorphism of materials can be a complete field of study. The macroscopic properties of a chemical compound depend on how the atoms interact at the microscopic level, and so the study of the structural arrangements which are the result of transforming the crystal form is the first step to understand and control those properties. The Raman spectrum acts as a fingerprint for both purity in chemical composition and crystal structure of one compound [1, 2], and so it can be extensively used for characterizing new materials and phase transitions as the works in Refs. [3, 4, 5, 6, 7, 8] show. Even though both, infrared (IR) and Raman spectroscopy probe the interatomic interactions through the phononic modes of vibration, in the oxides, the IR active modes are in general broader and impose bigger data treatment to extract their positions when compared to Raman spectroscopy. Thus, to follow the modification of phonon modes from one material to another or from the responses to one or other external parameter in these materials, Raman spectroscopy is more suitable. Moreover, Raman spectra do not suffer interference from extrinsic factors as the humidity of the environment, and it does not need an extensive sample preparation or exposition time, thus letting process and classify several samples in a short period of time. Here we will study the vibrational spectrum of some transition-metal oxides of the family MB_2O_6 (M and B are divalent and pentavalent cations, respectively) crystallised in a new structural form which is not conventional for these compounds.

When B =V in the formula MB_2O_6, these compounds are part of the so called "vanadate" phases. When synthesised at room pressure these vanadates

are found to adopt low symmetry structures such as triclinic $P\overline{1}$ for M =Cu, Ni or monoclinic $C2/m$ for M =Mg, Mn, Cd and Zn [9, 10]; when M =Co the structure can be triclinic or monoclinic depending on the temperature of synthesis [11, 12, 13]. By high pressure and temperature (HPHT) synthesis, some of these vanadates can be obtained in an orthorhombic structure with the *Pbcn* space group [14, 15, 16]; this is the columbite-type structure, typical of the room-pressure synthesised niobates (MB_2O_6, B =Nb). Previously, we reported the first Raman spectrum for the *Pbcn* NiV_2O_6 [16], and here we report the Raman spectra of *Pbcn* MnV_2O_6, CoV_2O_6 and ZnV_2O_6. To the best of our knowledge, this is the first report on the Raman spectra of these compounds crystallised in this specific structure. As we will expose below in this manuscript, different ions in the M position confer different physical properties that imply different uses for each of these compounds. With this study, we intend to explore the differences observed on the Raman spectrum when the M position is occupied by ions of magnetic (mainly Co and Ni) and not magnetic nature (Zn). Here, it is also possible to verify if the changes provoked in the interatomic vibrations by ions with different atomic numbers and electronic distribution are or not systematic which can be useful at the time of tuning properties for specific technological applications.

The columbite structure is formed by chains of oxygen octahedra surrounding both the M^{+2} and B^{+5} cations which run along the crystallographic c axis. Along the a axis, the MO_6 and BO_6 octahedra are stacked in a sequence $M - B - B - M$ as shown in Fig. 1 for the case M =Co. The oxygen atoms are located in the structure at one of the three non-equivalent positions, O_1, O_2, O_3, signaled by different colors in Fig. 1, and three types of B−O bonds can be distinguished [17]:

- Chain-type: bonding between two BO_6 octahedra belonging to different chains.
- Bridge-type: bonding between two BO_6 octahedra along one chain.
- Terminal-type: bond between one BO_6 and one MO_6 octahedra.

As it can be seen in the right inferior corner of Fig. 1, in the columbite structure the VO_6 octahedra are formed by one bond of terminal-type (V-O_t), two of bridge-type (V-O_b), and three of chain-type (V-O_c). The distortion of these octahedra can be measured by the polyhedral distortion index which is defined in Ref. [18, 19] as $\Delta = n^{-1}\sum_i^n(\frac{d_i-\overline{d}}{\overline{d}})^2$; n is the coordination number of the polyhedron central atom ($n = 6$ in our case), and $\overline{d}$ is the mean distance between the central atom (M or V) and its first neighbors, i.e. the oxygen atoms forming the octahedron.

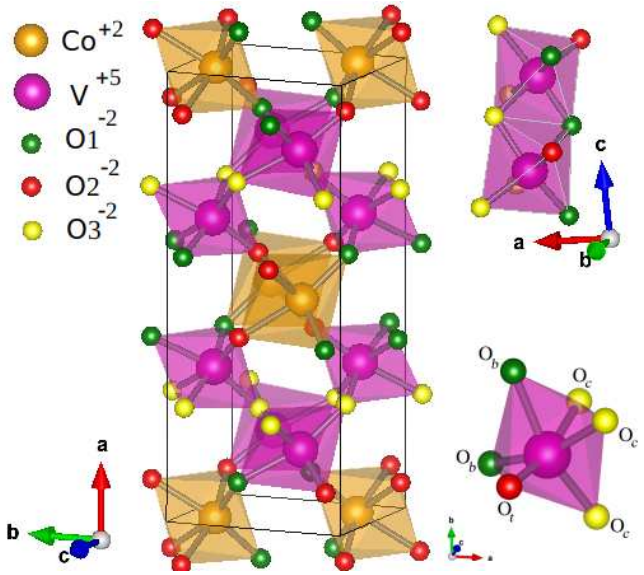

Figure 1: Unit cell of columbite-CoV_2O_6. Note the stacking Co-V-V-Co along the a axis. The small figure at top-right shows the chain of VO_6 octahedra along the c axis; the polyhedron at low-right shows the VO_6 octahedron with oxygen atoms forming bonds of type terminal, O_t, bridge, O_b, or chain, O_c (see text) drawn in red, green and yellow, respectively.

Vanadium is a multivalent metal that forms a large number of different stable oxides and metastable phases with a huge range of technological applications [20]. Among the transition metal vanadates, monoclinic MnV_2O_6 [21] has been investigated with success in the search for a single band-gap material that absorbs visible light and efficiently drives the photocatalytic hydrogen and oxygen production from hydrolysis. Recent studies on the triclinic form of NiV_2O_6 have also proved it as a visible- light-active photoanode for photoelectrochemi-

cal (PEC) water oxidation [22]. The monoclinic forms of MnV_2O_6 and ZnV_2O_6, this last in micro/nanostructures, have been synthesized as anode materials for lithium batteries [23, 24]. Besides, nanosheets of ZnV_2O_6 allow an enhanced photocatalytic CO_2 reduction with H_2O to solar fuels [25]. It can be inferred from the results in Ref. [26] that, while keeping ambient temperature, these properties of the of ZnV_2O_6 could be exploited at pressures up to 15 GPa since its monoclinic *C2/m* crystal structure remains stable at least up to that value; at higher pressures, Tang *et al.* showed that a *C2* phase appears to coexist with the *C2/m* ZnV_2O_6 when the pressure is kept between 16.6 and 16.9 GPa, and it is only *C2* at pressures $P \gtrsim 17$ GPa [5], where probably some of the physical properties are modified. To finish, studies on the magnetic properties of both monoclinic and triclinic forms of CoV_2O_6 propose it as a suitable material for magnetic refrigeration due to its larger magnetic entropy and adiabatic temperature change when submitted to magnetic fields of moderate intensity [27]. Motivated by this rich phenomenology, we present here the first study on the atomic vibrations spectra in a new structural phase of these oxide vanadates; with this we hope motivating further research on the physical phenomena occurring in these compounds and their possible uses.

2. Experimental details

Polycrystalline samples of MV_2O_6 (M =Mn, Co, Ni, Zn) with columbite-type crystal structure were produced by submitting pure-phase precursor powders with the same chemical formula of the products to temperatures between 700 and 900 ℃ and pressures between 5.5 and 6.7 GPa in presses of Belt and Conac types [28]. The specific synthesis conditions for each sample are presented in Table 1. In all cases the processing was done in 60 min at the maximal temperature and pressure followed by a rapid cooling to room temperature.

The structure of the samples was probed by reducing them to a fine powder to perform powder X-ray diffraction (XRD) measurements at room temperature. For samples with M =Co and Ni the measurements were performed in a

Table 1: Synthesis parameters used to obtain samples of MV_2O_6 in the *Pbcn* phase. The space group of the precursor powder (Precursor sym.) is indicated in each case.

M	Precursor sym.	P (GPa)	T (°C)
Mn	$C2/m$	5.8	800
Co	$P\bar{1}$	5.5	700
Ni	$P\bar{1}$	5.9	900
Zn	$C2/m$	6.7	900

Bruker D8 Endeavor diffractometer in the Bragg-Brentano geometry; for samples with M =Mn and Zn, these were done in a Siemens D5000 diffractometer in transmission geometry. In both cases, bichromatic Cu-$K_{\alpha 1,2}$ radiation was used. To obtain the structural parameters, the diffraction patterns were refined using FULLPROF program [18] by using the Rietveld method and considering pseudo-Voigt shaped peaks. The used refinement method followed the procedure described in Ref. [29] The figures showing the crystalline structure were made in VESTA [30] using the atomic position parameters derived from the Rietveld analysis.

The micro-Raman measurements were carried out at room temperature and pressure in a custom-built spectrometer at the "Institut Néel". The monochromator used was an ACTON Spectra Pro 2750 with a 1800 mm^{-1} grating blazed at 500 nm and a Pylon eXcelon CCD camera with 50 μm entrance slit providing a resolution of 0.03 nm, or 1.09 cm^{-1}; a set of three Bragg filters BNF-Optigrate was used in order to reject the excitation of the 514.4 nm (Cobolt Fandango) laser. The spectra were recorded in backscattering geometry with a 40x objective used both to focus the incident laser beam and to collect the scattered light. The spectrometer was calibrated in wavenumber by using the lines 540.056, 585.249, 588.190, 594.483 and 597.553 nm of the Princeton-Instrument Ne-Ar lamp. The measurements were carried out with a laser power of around $W \sim 0.6$ mW; this value was measured on the collimated laser beam before the objective with a silicon power head calibrated at 514 nm. The laser power was set in order to avoid any influence of laser heating on the Raman spectra. This

was done by monitoring that not visible changes with time were observed in the spectrum while the data were being acquired, and by verifying the reproducibility of the spectrum when measured at different values of the laser power. The samples with M =Mn, Co, were measured by performing a mean of two acquisitions of 120 s each. In the case M =Ni we used two frames of 240 s each, and in the case M =Zn three frames of 205 s were taken. In all cases measurements at several spots on the sample were taken in order to assure that the spectra were reproducible.

3. Results and discussion

The Rietveld refinement of the XRD data was completed in all cases by including only one columbite-type structural phase. The cell parameters and their standard deviation deduced from Rietveld refinements as defined in Ref. [31] are reported in Table 2. Note that the parameters reported here are the ones that serve to interpret the Raman spectroscopy data, which will be presented further in this manuscript. A more complete set of structural information for orthorhombic MnV_2O_6 and NiV_2O_6 is in Refs. [15] and [16], respectively, while the atomic positions and other structural parameters for orthorhombic CoV_2O_6 and ZnV_2O_6 will be reported elsewhere. Among the three cell parameters of the orthorhombic cell, the main change occurs along the a axis which reduces by 3.1% between the vanadate with M =Mn and the one with M =Ni. The lengths of the b and c axes reduce by around 1.3% when going from MnV_2O_6 to NiV_2O_6 while the volume of the cell reduces by 5.6%. The values of ionic radii calculated in Ref. [32] for divalent cations with coordination number six are 0.83, 0.75, 0.69 and 0.74 Å for Mn^{+2}, Co^{+2}, Ni^{+2} and Zn^{+2}, respectively; then, Mn^{+2} and Ni^{+2} correspond to the two extreme values of ionic radius of the series studied here and so the reduction of the cell volume can be explained. However, it is curious to observe that the length of the a and $b-$axes, and the volume of the cell, depend linearly not on the ionic, but on the covalent radius of cation M (r_M) as it is shown in Fig. 2.

Table 2: Cell parameters of the studied samples of MV_2O_6 (M = Mn, Co, Ni, Zn) crystallised in the *Pbcn*-space group. The data are derived from room temperature XRD patterns. The errors are the statistical ones coming from the Rietveld refinement; experimental errors are not included.

M	Mn	Co	Ni	Zn
a (Å)	13.7722(7)	13.4785(2)	13.3518(2)	13.590(2)
b (Å)	5.6004(3)	5.5495(1)	5.5252(1)	5.6012(9)
c (Å)	4.8779(3)	4.8344(1)	4.8145(1)	4.8371(8)
Vol (Å^3)	376.24(4)	361.61(1)	355.166(8)	368.2(1)
R_P (%)	6.6	6.16	9.71	18.7
R_{WP} (%)	8.1	7.85	12.4	9.2

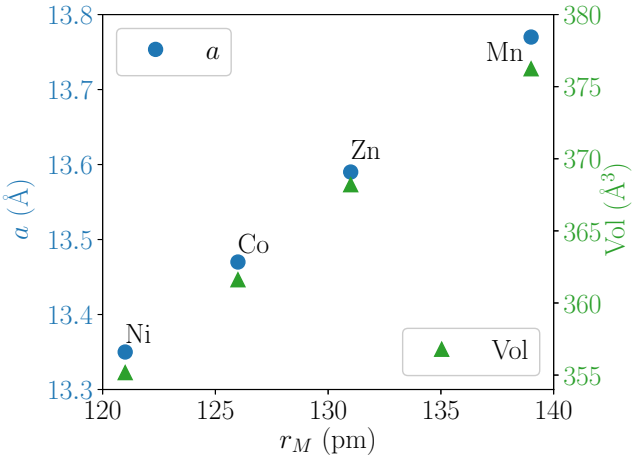

Figure 2: Evolution of the unit cell size with covalent radius of atom M. Statistical errors are below the size of the markers.

Table 3: Interatomic V-O, and $M-$O, distances in the columbite-type MV_2O_6 samples studied here. O_t, O_b, and O_c correspond to oxygen atoms in position terminal, bridge, and chain, respectively (see text for more details). The distortion indexes $\Delta_{V,M}$ of the VO_6 and MO_6 octahedra are also presented.

M	Mn	Co	Ni	Zn
$d_{\text{V-O}_t}$ (Å)	1.47(1)	1.75(3)	1.65(2)	1.77(7)
$< d_{\text{V-O}_b} >$ (Å)	1.97(2)	1.93(4)	1.92(2)	2.09(2)
$< d_{\text{V-O}_c} >$ (Å)	1.96(2)	1.97(4)	1.97(4)	1.96(2)
Δ_{V} (10^{-3})	10.7(1)	4.3(1)	7.0(1)	15.0(1)
$< d_{M\text{-O}} >$ (Å)	2.264(3)	2.046(8)	2.073(7)	2.04(3)
Δ_M (10^{-3})	6.3(1)	0.8(1)	0.1(0)	6.2(1)

We calculated the set of interatomic distances and distortion indexes Δ reported in Table 3 which are useful to interpret the data. For the VO_6 octahedra the reported interatomic distances are: the distance between the vanadium atom at the center and the oxygen atom in the terminal position, $d_{\text{V-O}_t}$, the mean distance of the two V-O_b bonds, $< d_{\text{V-O}_b} >$, and the mean distance of the three V-O_c bonds, $< d_{\text{V-O}_c} >$. For the MO_6 octahedra, the reported value is the mean distance between the central $M-$cation and its six first neighbor oxygen atoms, $< d_{M\text{-O}} >$.

Looking at the values reported in Table 3, one can note that taking into account the error, distances $< d_{\text{V-O}_c} >$ and $< d_{\text{V-O}_b} >$ remain essentially the same for all cations M. On the other hand, $d_{\text{V-O}_t}$ show variations which do not change systematically with the ionic radius of the cation M. This non-systematic variation is also observed in distance $< d_{M\text{-O}} >$; however, it is interesting to note that the variation of $< d_{M\text{-O}} >$ is opposite to the one observed in $d_{\text{V-O}_t}$. This puts in evidence the influence of the cation M on the V-O bonds, specially on the V-O_t one. In addition, the distortion indexes of the octahedra, Δ_V and Δ_M indicate that the octahedral units of the vanadates MV_2O_6 in the *Pbcn* structure exhibit a more regular shape when M =Co or Ni than when M = Mn or Zn. In the case of $M = Mn^{+2}$ it is straightforward to think that there is a cost on the symmetry of the basic units of the structure to accommodate such a large ion. As seen in the previous paragraph, the ionic size of Zn^{+2} is almost

the same than that of Co^{+2} (~ 0.75 Å) and so the penalty in distortion index of the VO_6 and MO_6 octahedra in the ZnV_2O_6 with respect to CoV_2O_6 must be due to different physicochemical factors.

The measured Raman spectra for the *Pbcn* MnV_2O_6, CoV_2O_6, NiV_2O_6 and ZnV_2O_6 are presented in Fig. 3. From top to bottom the mass of M cation tends to increase whereas its size decreases from M =Mn to M =Ni and it increases again for M =Zn [32]. The spectra for samples with M =Mn, Co and Zn are reported for the first time, while that for M =Ni is recalled from our previous work recently published in Ref. [16]. We can first observe in Fig. 3 that the four recorded Raman spectra present strong similarities both in the position in wavenumber ($\bar{\omega}$) of bands as well as in their intensity. In all cases the tallest peak occurs in the region $\bar{\omega} \geq 500$ cm^{-1} and, as it is much taller than any of the peaks in the region $\bar{\omega} < 500$ cm^{-1}, these two regions are presented separately in Fig. 3, and the vertical axis is normalised to the height of the tallest peak in each region. In the low-wavenumber part of the spectra, even if we expect to observe many Raman modes that can make difficult to follow a specific mode, the global shape is preserved and it is still possible to identify modes which are common to all spectra independently of the cation M.

From group theory and atomic positions in the MB_2O_6 compounds (atom M Wyckoff position 4c, atoms B and O Wyckoff position 8d) with columbite structure, we expect 54 Raman active modes distributed in 13 symmetric modes (A_g), and 41 asymmetric modes (14 modes B_{1g}, 13 modes B_{2g} and 14 modes B_{3g}). This calculation was performed by Husson *et al.* in Ref. [17] by following the Bhagavantam method described in its internal reference number eighteen. We investigated the 7 most intense Raman modes, mainly of symmetry A_g, that could unequivocally be identified as common in the spectra of all the four samples; these are presented in Table 4 (a tentative identification of another modes are presented in the supplementary file). The frequency reported in Table 4 for the Raman peaks is the one corresponding to the point of maximum intensity of each peak. For ZnV_2O_6, the Raman signature of its different polymorphs was investigated by ab-initio calculations in Ref. [33]. When we compare, the posi-

tion of the modes for the orthorhombic *Pbcn* structure coincides approximately with the experimentally found by us for the modes in the region $\bar{\omega} < 500$; however, in the higher wavenumbers region, neither the intensity or the position of the predicted Raman modes, which are shifted by more than 70 cm^{-1}, agree with the experimentally observed spectrum. At this point, it is of worth to say that we are able to identify common characteristics in the spectra of our ZnV_2O_6 sample with the other three measured ones, and specially with that reported in Ref. [34] for columbite MgV_2O_6, and so we can be sure that the experimentally recorded spectrum is the true spectrum of the columbite phase of ZnV_2O_6. A discrepancy between theoretically calculated and experimentally observed values for the Raman modes is actually expected since the calculations are performed in interaction free environments which are not the ones found in real compounds. Additional sources of discrepancy between the theoretical calculations and the experiments probably come from the differences in the calculations of the cell parameters and the interatomic distances, mainly in the length of the a parameter and $d_{\text{V-O}_t}$, which, as it will be commented below, is responsible for the vibrations at the higher wavenumbers region of the Raman spectrum. The same shift at high wavenumbers was observed in the main text of Ref. [33] for the *C2/m* polymorph of ZnV_2O_6; thus indicating that the *ab initio* calculations can have a bias at high wavenumber in both *C2/m* and *Pbcn* structures.

The infrared and Raman spectra of the columbite-type niobates $M\text{Nb}_2\text{O}_6$ was rigorously studied, theoretically and experimentally, by Husson *et al.* in a series of articles [17, 35, 36]. Thus, taking into account that the niobates are of the same family of oxides and have the same crystal structure than the samples we are studying here, we took those studies as a basis to make the assignment of the vibrations corresponding to the Raman peaks observed in our samples. As in the niobates, it is expected that the peaks at the highest wavenumbers ($\bar{\omega} \gtrsim 500$ cm^{-1}) in the vanadates are related to stretching vibrations of the VO_6 octahedra implying oxygen atoms mainly located in the bridge or terminal positions. At lower wavenumbers ($100 < \bar{\omega} < 500$ cm^{-1}) the peaks observed

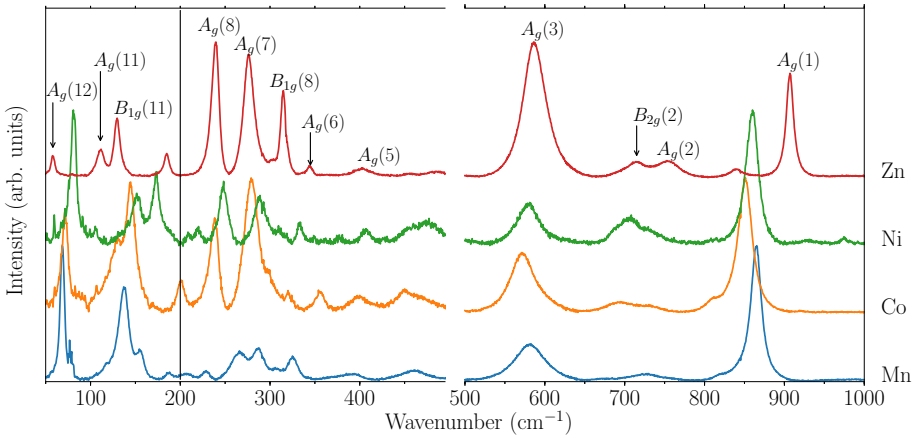

Figure 3: Raman spectra for all the studied samples of $M\mathrm{V_2O_6}$. The vertical axis is normalized by the most intense peak in each of the two separated regions $0 \leq \bar{\omega} \leq 500$ cm^{-1} and $\bar{\omega} > 500$ cm^{-1}. The vertical solid line at $\bar{\omega} \sim 200$ cm^{-1} separates the region where the lattice vibrations manifest.

Table 4: Position of some peaks identified in the Raman spectra of the $M\mathrm{V_2O_6}$ samples studied here. This position is given in units of the relative wavenumber $\bar{\omega}$ in cm^{-1}. The symmetry of the modes was found by comparison with the known spectrum of the isostructural compounds $M\mathrm{Nb_2O_6}$ (see text). Stretching and bending are written as "(st)" and "(bd)", respectively.

Mode	Mn	Co	Ni	Zn	Vibration
$A_g(1)$	864	850	859	906	V-O_t(st)
$A_g(3)$	581	571	579	586	V-O_b(st)
$A_g(7)$	265	279	288	276	O-M-O(bd) + V-O-M(bd) + V-V(st)
$A_g(8)$	229	238	249	239	
$B_{1g}(11)$	155	144	173	130	Lattice-related modes
$A_g(11)$	138	130	152	111	
$A_g(12)$	68	71	81	58	

in the spectra are due to bending modes and torsion modes that imply V-O_c bonds and displacements of the M cations. Finally, at very low values of the wavenumber ($\bar{\omega} < 100$ cm^{-1}) the modes that manifest are due to the relative vibrations of the M and V sub-lattices.

In the region $\bar{\omega} > 500$ cm^{-1}, the peaks $A_g(1)$ and $A_g(3)$ stand out and are easily recognizable in the spectra of all the four samples (see Fig. 3). The highest wavenumber peak, $A_g(1)$, appears in the niobates at $\bar{\omega} \sim$900 cm^{-1}. In the vanadates, this is the tallest peak of the spectrum for samples with M =Mn, Co, Ni, and it occurs at wavenumbers around $\bar{\omega} \sim 860$ cm^{-1} for those samples. For sample ZnV_2O_6, peak $A_g(1)$ occurs at a higher frequency, $\bar{\omega} \sim 906$ cm^{-1} and it exhibits a lower intensity than peak $A_g(3)$. This is also a characteristic of the Raman spectrum of *Pbcn* MgV_2O_6 reported in ref. [34].

The intense symmetric stretching mode observed at high frequency is not exclusive of the niobates and vanadates with stoichiometry 1:2:6; it is also observed in the Raman spectra of the rare-earth orthovanadates with chemical formula AVO_4 (A = Sm, Ho, Yb, Lu, Tb, Nd) [37, 38, 39]. In those compounds the $A_g(1)$ peak appears at frequencies between ~ 870 and ~ 920 cm^{-1}, and it is related to internal VO_4 bonds [39]. In those compounds, the frequency of the internal VO_4 vibrations increases with the mass of the ion A because the A-O distances decrease as **Z** increases; it is interpreted as an increase in the force constant of the atomic bonds in the VO_4 tetrahedron as the A ion changes. In the case of the AB_2O_6 vanadates investigated by us, the highest wavenumber mode, $A_g(1)$, is also related to the vibration of the V-O_t bond; however, changes in the size and shape of the VO_6 octahedra induced by the M cations does not produce the changes in wavenumber of mode $A_g(1)$ that are predicted by the Badger rule. With increasing atomic number **Z**, $d_{\text{V-O}_t}$ increases from 1.47 to 1.76 Å when passing from M =Mn to Co, then it decreases to 1.64 Å when M =Ni, and finally it increases up to 1.77 Å when M =Zn. From the Badger's rule it is expected that shorter interatomic distances produce higher wavenumbers for the Raman peaks. The plot of $\bar{\omega}^{2/3}$ for the position in wavenumber of mode $A_g(1)$ as a function of the inverse of $d_{\text{V-O}_t}$ is presented in Fig. 4.

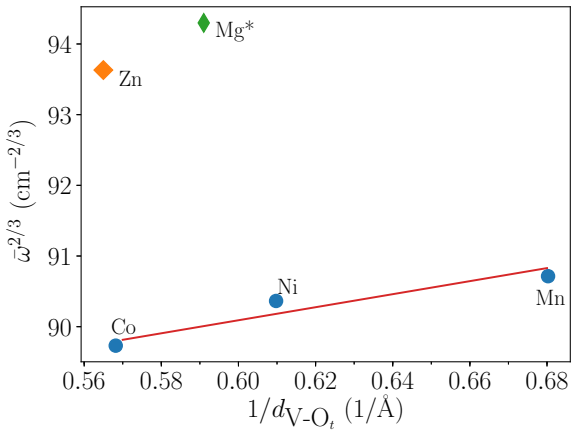

Figure 4: Variation of the position of the Raman mode $A_g(1)$ with the inverse of the distance of the V-O_t bond in a series of vanadates MV$_2$O$_6$ crystallized in the *Pbcn* space group. The solid, red line evidences that the points corresponding to M =Mn, Co, and Ni approximately follow the Badger's rule. *The data for M =Mg were taken from Ref. [34]. Errors are the size of the points.

There, it is revealed that the classical Badger's rule is approximately obeyed in the columbites MV$_2$O$_6$ when M =Mn, Co and Ni but not when M =Zn or Mg which exhibits a far too high wavenumber position. This result implies the effect of additional factors, others than only the geometrical ones, determining the position of the Raman peaks of the $A_g(1)$ mode along the series of vanadates MV$_2$O$_6$ when crystallized in the columbite form.

The unexpected results described in the precedent paragraph with respect to the position of peak $A_g(1)$ in the Raman spectra of ZnV$_2$O$_6$ and MgV$_2$O$_6$ reveals the effect of the cation M on the force constant of the V-O_t bond. This influence is probably related to electronic more than geometric factors as pointed before by the similar effects already observed in the series of niobates MNb$_2$O$_6$ studied in Ref. [35] and in some polymorphs of ZnV$_2$O$_6$ under hydrostatic pressure [33]. In Ref. [33] a pressure-induced mechanism of charge transference from the ZnO$_6$ to the VO$_6$ octahedra was used to explain the influence of the electronic properties of Zn^{+2} in the position of the Raman modes attributed to vibrations only involving V^{+5} and O^{-2} atoms, and so the violation of Badger's relation when a pressure of 30 GPa was applied to the monoclinic

forms (*C2/m, C2, C2/c*) of the ZnV_2O_6. Similarly, in Ref. [35] it was found that in the MNb$_2$O$_6$ compounds, the Nb-O$_t$ bond is easily influenced by the exterior electrostatic field and so its force constant reduces linearly with the electronegativity of the cations M [35]. In this way, cations M with higher electronegativity tend to reduce the wavenumber where the mode $A_g(1)$ is observed along one series of MNb$_2$O$_6$ compounds. In summary, we can assume that both in the monoclinic and columbite forms of the M(Nb,V)$_2$O$_6$ compounds, the position in wavenumber of the modes related only to Nb/V and O atoms (mode $A_g(1)$ in the columbites) depend both on the (Nb/V)-O$_t$ distance and the electronegativity of cation M. Taking this into account, and assuming that the difference between the electronegativity of the cations is the same than that in the neutral atoms, the increase in wavenumber of the mode $A_g(1)$ observed here in the columbites MV$_2$O$_6$ when passing from M =Ni to M =Zn can be explained by the reduction of the electronegativity which goes from 1.91 in Ni to 1.65 in Zn. This argument also applies when we include in our analysis the data reported in Ref. [34] for the *Pbcn*-MgV$_2$O$_6$. In that case the mode $A_g(1)$ was observed at $\bar{\omega} \sim 915$ cm^{-1}, while the reported V-O$_t$ distance is 1.692 Å. That wavenumber is approximately 50 cm^{-1} higher than the wavenumber observed by us for the MnV$_2$O$_6$, even though the reported distance of the V-O$_t$ bond is larger (see Table 3); however, the electronegativity of the Mg is 15% smaller than that of the Mn and so it can be responsible for the step increase in the frequency of the $A_g(1)$ mode in MgV$_2$O$_6$ with respect to the MnV$_2$O$_6$.

The difficulty of interpreting the variation of the position of the $A_g(1)$ mode only with basis on the interatomic distances of the V-O$_t$ bond in the columbites MV$_2$O$_6$ had also been evidenced in the analysis of the whole series of samples NiNb$_{2-x}$V$_x$O$_6$ studied in Ref. [16]. There, it was concluded that the relative wavenumber of the highest intensity Raman peak is very sensitive to the specific details of the crystalline structure as a whole and apparently this mode tends to appear at lower wavenumbers in more symmetric structures. We corroborate that result for all samples studied here as can be seen in Fig. 5. This result lead us to deduce that the lower distortion index Δ_V calculated for MnV$_2$O$_6$

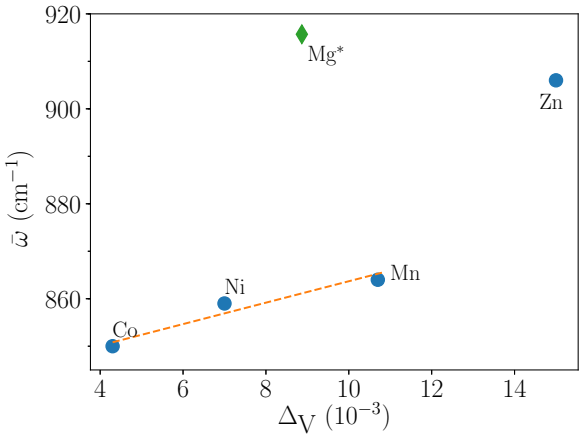

Figure 5: Variation of the position of the mode $A_g(1)$ with the distortion index of the VO_6 octahedra, Δ_V , in a series of MV_2O_6 compounds crystallised in the columbite-type structure. *The point for M =Mg was calculated from data in Ref. [34]. Errors are the size of the points.

with respect to that of ZnV_2O_6 (see Table 3) could be responsible for reducing the wavenumber of mode $A_g(1)$ in the former with respect to the last one even though $d_{V\text{-}O_t}$ is smaller in MnV_2O_6 than in ZnV_2O_6. When we include the point for one sample of *Pbcn*-MgV_2O_6 calculated from data in Ref. [34], a trend similar to that observed in Fig. 4 appears in the sense that Mg and Zn seem to conform to a different group of compounds. The characteristic that makes them different from the compounds with M =Mn, Co and Ni is maybe in the specific characteristics of the electronic structure, for example, the fact of having closed shells of electrons, $2p^6$ in the case of Mg^{+2} and $3d^{10}$ in the case of Zn^{+2}.

Still in the region $\bar{\omega} \geq 500$ cm^{-1} we observe the mode $A_g(3)$. This mode is observed at $\bar{\omega} \sim 580$ cm^{-1} is mainly ruled by the stretching of the bonds V-O_b [35, 36]. However as here we see that it displays the same dependence with M cation that the mode $A_g(1)$, we could think that it is also sensitive to the V-O_t bond and so to the electronegativity of the M cation. However in this case the effect is less pronounced than in the case of $A_g(1)$ because the force constant of the V-O_b bonding is less sensible to the surrounding electric field than that of the V-O_t bonding [35].

With respect to the isostructural columbite-niobates, $M\mathrm{Nb_2O_6}$, the mode $A_g(1)$ is observed at higher wavenumbers in those compounds than in the vanadates $M\mathrm{V_2O_6}$ when M =Mn [35], Co (own measure, not shown), and Ni [16]. In contrast, the frequency of the mode $A_g(1)$ reported for the $\mathrm{ZnNb_2O_6}$ in Ref. [35] is ~ 13 cm^{-1} lower than the one measured by us for the columbite $\mathrm{ZnV_2O_6}$. On the other hand, the mode $A_g(3)$ is always observed at lower wavenumbers in the niobates than in the respective vanadates. Nevertheless, the variation in wavenumber of the peak $A_g(1)$ when going from one cation M to another is the same along the series of vanadates than along the series of niobates. All these facts show that in the columbite compounds of the $MB_2\mathrm{O_6}$ family, both geometrical and physicochemical factors have to be taken into account in order to explain the position of the Raman peaks.

In the region $\bar{\omega} < 500$ cm^{-1}, the position in wavenumber of modes $A_g(7)$ and $A_g(8)$ increases with $\mathbf{Z}$ when going from M =Mn to M =Ni, and then it reduces when going from M =Ni to M =Zn, i.e. they display the same tendency of $1/< d_{\mathrm{V\text{-}O}_b} >$ or the inverse of the cell volume or the electronegativity of cations M. This reveals that these modes are connected with VO_b chain bounds through global octahedra chain in the orthorhombic structure. As the lower wavenumber modes are generally associated to M and V lattices modes, they should be the ones to be influenced by the change of the mass of the M cations. The Mn, Co and Ni have masses which are quite close with a slight increase from Mn to Co or Ni. However the Zn mass is 19% larger than that of Mn. This mass effect is clearly observed for the modes with wavenumber lower than 200 cm^{-1} i.e. $A_g(12)$ $A_g(11)$, and $B_{1g}(11)$. Because the global volume is reduced we can expect that the $M - M$ distance will decrease also and thus the increase of wavenumber from Mn to Co and Ni is reflecting this cell contraction because the mass is roughly the same for these cations.

4. Conclusions

We present here the first report on the Raman spectra of the oxide-vanadates MnV_2O_6, CoV_2O_6 and ZnV_2O_6 crystallized in the columbite-type structure. We succeed to have one single structural phase of all these compounds by synthesis in extreme conditions of high pressure and temperature. In order to have a more complete set of data, we also present data for the columbite NiV_2O_6 and so we were able to identify the characteristics that are common in the Raman spectra of all these compounds. Thanks to this systematic comparison of the vanadates Raman spectra, several peaks were assigned ranging from bending and stretching modes of vibration of the V-O and $M-$O bonds present in the columbite structure. We could see that the force constants of both the V-O_t and V-O_b bonds are strongly influenced by the force constant of the $M-$O bonds. It is probably the interplay between geometric and electronic factors that makes that the $M-$O distance does not vary linearly with the electronegativity of the cation M. This is a crucial difference between the niobates and the vanadates of the AB_2O_6 family and could be the basis to analyze the subsequent differences in physical properties among these two series of compounds.

In the higher wavenumber region of the Raman spectra ($\bar{\omega} > 500$ cm^{-1}) the evolution of the Raman peaks with the atomic number of cation M is ruled by both electronic and structural factors. The changing in the position of mode $A_g(1)$ with different M reveals the strong influence of the electronegativity of cation M in the force constant of the V-O_t bonds. Another important factor that rules the position of mode $A_g(1)$ is the symmetry of the VO_6 octahedra; less distorted octahedra reduce the wavenumber where mode $A_g(1)$ is observed. At wavenumbers $\bar{\omega} < 500$ cm^{-1} several of the identified modes behave according to the expected by the change in mass of cation M.

The analysis of the Raman spectra gives information about the influence of some specific chemical characteristics can open the door for studying of new physical interesting properties, specifically the optical ones which have been the most studied recently. We hope that the present study will stimulate some

theoretical work to predict the full Raman spectrum of this new MV_2O_6 series of compounds and that the results described above will add some value to the previously reported Raman spectroscopy investigations for other *Pbcn* oxide vanadates thus helping to the understanding of such complex spectra.

5. Acknowledgments

This work was financed by the french-brazilian cooperation program "CAPES-COFECUB", process 88887.321681/2019-00, and the french institution "Centre National de la Recherche Scientifique", CNRS. Funding for this project was provided by a grant from Région Rhône-Alpes (MIRA scholarship). The present work was also partially supported by the Brazilian agency Conselho Nacional de Desenvolvimento Científico e Tecnológico - CNPq." We thank to the professional team of the X-Press pole of the "Institut Néel", specially to Murielle Legendre for the technical support in the preparation of the samples.

References

References

[1] R. R. Jones, D. C. Hooper, L. Zhang, D. Wolverson, V. K. Valev, Raman Techniques: Fundamentals and Frontiers, Nanoscale Research Letters 14 (1) (2019) 231. doi:10.1186/s11671-019-3039-2.

[2] R. Loudon, The raman effect in crystals, Advances in Physics 13 (52) (1964) 423–482. arXiv:https://doi.org/10.1080/00018736400101051, doi:10.1080/00018736400101051.
URL https://doi.org/10.1080/00018736400101051

[3] P. Bouvier, J. Kreisel, Pressure-induced phase transition in $LaAlO_3$, Journal of Physics Condensed Matter 14 (15) (2002) 3981–3991. doi:10.1088/0953-8984/14/15/312.

[4] P. Bouvier, J. Godlewski, G. Lucazeau, A Raman study of the nanocrystallite size effect on the pressure temperature phase diagram of zirconia grown by zirconium-based alloys oxidation, Journal of Nuclear Materials 300 (2) (2002) 118–126. doi:10.1016/S0022-3115(01)00756-5.

[5] R. Tang, Y. Li, D. Han, H. Li, Y. Zhao, C. Gao, P. Zhu, X. Wang, A Reversible Structural Phase Transition in ZnV_2O_6 at High Pressures, The Journal of Physical Chemistry C 118 (20). doi:10.1021/jp411283m.

[6] Y. Li, R. Tang, N. Li, H. Li, X. Zhao, P. Zhu, X. Wang, Pressure-induced amorphization of metavanadate crystals SrV_2O_6 and BaV_2O_6, Journal of Applied Physics 118 (3) (2015) 035902. arXiv:https://doi.org/10.1063/1.4926784, doi:10.1063/1.4926784. URL https://doi.org/10.1063/1.4926784

[7] R. Tang, Y. Li, S. Xie, N. Li, J. Chen, C. Gao, P. Zhu, X. Wang, Exploring the coordination change of vanadium and structure transformation of metavanadate MgV_2O_6 under high pressure, Scientific Reports 6 (2016) 38566. doi:10.1038/srep38566.

[8] F. Huang, Q. Zhou, L. Li, X. Huang, D. Xu, F. Li, T. Cui, Structural Transition of $MnNb_2O_6$ under Quasi-Hydrostatic Pressure, The Journal of Physical Chemistry C 118 (33) (2014) 19280–19286. arXiv:https://doi.org/10.1021/jp503542y, doi:10.1021/jp503542y. URL https://doi.org/10.1021/jp503542y

[9] M. L. Hneda, J. B. M. da Cunha, A. Popa, O. Isnard, Magnetic order suppression and structural characterization of $MnNb_{2-x}V_xO_6$ columbites crystallized under extreme pressure conditions, Journal of Magnetism and Magnetic Materials 496 (2020) 165907. doi:10.1016/j.jmmm.2019.165907.

[10] E. J. Baran, C. I. Cabello, A. G. Nord, Raman spectra of some MV_2O_6 brannerite-type metavanadates, Journal of Raman Spectroscopy 18 (6) (1987) 405–407. doi:10.1002/jrs.1250180606.

[11] M. Markkula, A. M. Arevalo-Lopez, J. Paul Attfield, Neutron diffraction study of monoclinic brannerite-type CoV_2O_6, Journal of Solid State Chemistry France 192 (2012) 390–393. doi:10.1016/j.jssc.2012.04.029.

[12] M. Lenertz, J. Alaria, D. Stoeffler, S. Colis, A. Dinia, O. Mentré, G. André, F. Porcher, E. Suard, Magnetic structure of ground and field-induced ordered states of low-dimensional α-CoV_2O_6: Experiment and theory, Phys. Rev. B 86 (21) (2012) 214428. doi:10.1103/PhysRevB.86.214428.

[13] D. Von Dreifus, R. Pereira, A. D. Rodrigues, E. C. Pereira, A. J. A. de Oliveira, Sol-gel synthesis of triclinic CoV_2O_6 polycrystals, Ceramics International 44 (16) (2018) 19397 – 19401. doi:https://doi.org/10.1016/j.ceramint.2018.07.171.
URL http://www.sciencedirect.com/science/article/pii/S0272884218319114

[14] M. Gondrand, A. Collomb, J. C. Joubert, R. D. Shannon, Synthesis of new high-pressure columbite phases containing pentavalent vanadium, Journal of Solid State Chemistry France 11 (1) (1974) 1–9. doi:10.1016/0022-4596(74)90139-X.

[15] M. L. Hneda, J. B. M. da Cunha, M. A. Gusmão, S. R. O. Neto, J. Rodríguez-Carvajal, O. Isnard, Low-dimensional magnetic properties of orthorhombic MnV_2O_6 : A nonstandard structure stabilized at high pressure, Phys. Rev. B 95 (2) (2017) 024419. doi:10.1103/PhysRevB.95.024419.

[16] J. P. Peña, P. Bouvier, O. Isnard, Structural properties and Raman spectra of columbite-type $NiNb_{2-x}V_xO_6$ synthesized under high pressure, Journal of Solid State Chemistry 291 (2020) 121607. doi:https://doi.org/10.1016/j.jssc.2020.121607.
URL http://www.sciencedirect.com/science/article/pii/S0022459620304370

[17] E. Husson, Y. Repelin, N. Q. Dao, H. Brusset, E. Fardouet, Etude par spectrophotométries d'absorption infrarouge et de diffusion Raman des nio-

bates de structure columbite, Spectrochimica Acta Part A: Molecular Spectroscopy 33 (11) (1977) 995–1001. doi:10.1016/0584-8539(77)80101-3.

[18] J. Rodríguez-Carvajal, Recent advances in magnetic structure determination by neutron powder diffraction, Physica B Condensed Matter 192 (1-2) (1993) 55–69. doi:10.1016/0921-4526(93)90108-I.

[19] I. D. Brown, R. D. Shannon, Empirical bond-strength–bond-length curves for oxides, Acta Crystallographica Section A 29 (3) (1973) 266–282. arXiv:https://onlinelibrary.wiley.com/doi/pdf/10.1107/S0567739473000689, doi:10.1107/S0567739473000689.
URL https://onlinelibrary.wiley.com/doi/abs/10.1107/S0567739473000689

[20] P. Shvets, O. Dikaya, K. Maksimova, A. Goikhman, A review of Raman spectroscopy of vanadium oxides, Journal of Raman Spectroscopy 50 (8) (2019) 1226–1244. doi:10.1002/jrs.5616.

[21] B. Zoellner, E. Gordon, P. A. Maggard, A small bandgap semiconductor, p-type MnV_2O_6, active for photocatalytic hydrogen and oxygen production, Dalton Trans. 46 (2017) 10657–10664. doi:10.1039/C7DT00780A.
URL http://dx.doi.org/10.1039/C7DT00780A

[22] H. X. Dang, A. J. E. Rettie, C. B. Mullins, Visible-Light-Active NiV_2O_6 Films for Photoelectrochemical Water Oxidation, The Journal of Physical Chemistry C 119 (26) (2015) 14524–14531. arXiv:https://doi.org/10.1021/jp508349g, doi:10.1021/jp508349g.
URL https://doi.org/10.1021/jp508349g

[23] S.-S. Kim, H. Ikuta, M. Wakihara, Synthesis and characterization of MnV_2O_6 as a high capacity anode material for a lithium secondary battery, Solid State Ionics 139 (1) (2001) 57 – 65. doi:https://doi.org/10.1016/S0167-2738(00)00816-X.
URL http://www.sciencedirect.com/science/article/pii/S016727380000816X

[24] Y. Sun, C. Li, L. Wang, Y. Wang, X. Ma, P. Ma, M. Song, Ultralong monoclinic ZnV_2O_6 nanowires: their shape-controlled synthesis, new growth mechanism, and highly reversible lithium storage in lithium-ion batteries, RSC Adv. 2 (2012) 8110–8115. doi:10.1039/C2RA20825C.
URL http://dx.doi.org/10.1039/C2RA20825C

[25] A. Bafaqeer, M. Tahir, N. A. S. Amin, Synthesis of hierarchical ZnV_2O_6 nanosheets with enhanced activity and stability for visible light driven CO_2 reduction to solar fuels, Applied Surface Science 435 (2018) 953 – 962. doi:https://doi.org/10.1016/j.apsusc.2017.11.116.
URL http://www.sciencedirect.com/science/article/pii/S0169433217333986

[26] D. Díaz-Anichtchenko, D. Santamaria-Perez, T. Marqueño, J. Pellicer-Porres, J. Ruiz-Fuertes, R. Ribes, J. Ibañez, S. Achary, C. Popescu, D. Errandonea, Comparative study of the high-pressure behavior of znv_2o_6, $zn_2v_2o_7$, and $zn_3v_2o_8$, Journal of Alloys and Compounds 837 (2020) 155505. doi:https://doi.org/10.1016/j.jallcom.2020.155505.
URL http://www.sciencedirect.com/science/article/pii/S0925838820318697

[27] M. Nandi, P. Mandal, Magnetic and magnetocaloric properties of quasi-one-dimensional Ising spin chain CoV_2O_6, Journal of Applied Physics 119 (13) (2016) 133904. arXiv:1509.01690, doi:10.1063/1.4945395.

[28] Press description, http://neel.cnrs.fr/equipes-poles-et-services/xpress, accessed: 2020-10-27.

[29] L. B. McCusker, R. B. Von Dreele, D. E. Cox, D. Louër, P. Scardi, Rietveld refinement guidelines, Journal of Applied Crystallography 32 (1) (1999) 36–50. doi:10.1107/S0021889898009856.
URL https://doi.org/10.1107/S0021889898009856

[30] K. Momma, F. Izumi, *VESTA3* for three-dimensional visualization of crystal, volumetric and morphology data, J. Appl. Cryst. 44 (6) (2011) 1272–

1276. doi:10.1107/S0021889811038970.
URL https://doi.org/10.1107/S0021889811038970

[31] R. A. Young, E. Prince, R. A. Sparks, Suggested guidelines for the publication of Rietveld analyses and pattern decomposition studies, Journal of Applied Crystallography 15 (3) (1982) 357–359. doi:10.1107/S0021889882012138.
URL https://doi.org/10.1107/S0021889882012138

[32] R. D. Shannon, Revised effective ionic radii and systematic studies of interatomic distances in halides and chalcogenides, Acta Cryst. 32 (1976) 751 – 767. doi:10.1107/S0567739476001551.

[33] A. Beltrán, L. Gracia, J. Andrés, Polymorphs of ZnV_2O_6 under Pressure: A First-Principle Investigation, The Journal of Physical Chemistry C 123 (5) (2019) 3239–3253. doi:10.1021/acs.jpcc.8b12515.
URL https://doi.org/10.1021/acs.jpcc.8b12515

[34] R. L. Tang, Y. Li, Q. Tao, N.-N. Li, H. Li, D. D. Han, P. W. Zhu, X. Wang, High-pressure Raman study of MgV_2O_6 synthesized at high pressure and high temperature, Chinese Physics B 22 (6) (2013) 066202. doi:10.1088/1674-1056/22/6/066202.

[35] E. Husson, Y. Repelin, N. Q. Dao, H. Brusset, Normal coordinate analysis of the MNb_2O_6 series of columbite structure (M=Mg, Ca, Mn, Fe, Co, Ni, Cu, Zn, Cd), J. Chem. Phys. 67 (3) (1977) 1157–1163. doi:10.1063/1.434968.

[36] E. Husson, Y. Repelin, N. Q. Dao, H. Brusset, Normal coordinate analysis for $CaNb_2O_6$ of columbite structure, J. Chem. Phys. 66 (11) (1977) 5173–5180. doi:10.1063/1.433780.

[37] C. C. Santos, E. N. Silva, A. P. Ayala, I. Guedes, P. S. Pizani, C. K. Loong, L. A. Boatner, Raman investigations of rare earth ortho-

vanadates, Journal of Applied Physics 101 (5) (2007) 053511–053511–5. doi:10.1063/1.2437676.

[38] D. Errandonea, F. Manjón, A. Muñoz, P. Rodríguez-Hernández, V. Panchal, S. Achary, A. Tyagi, High-pressure polymorphs of $tbvo_4$: A raman and ab initio study, Journal of Alloys and Compounds 577 (2013) 327 – 335. doi:https://doi.org/10.1016/j.jallcom.2013.06.008.
URL http://www.sciencedirect.com/science/article/pii/S0925838813014059

[39] V. Panchal, D. Errandonea, F. Manjón, A. Muñoz, P. Rodríguez-Hernández, S. Achary, A. Tyagi, High-pressure lattice-dynamics of ndvo4, Journal of Physics and Chemistry of Solids 100 (2017) 126 – 133. doi:https://doi.org/10.1016/j.jpcs.2016.10.001.
URL http://www.sciencedirect.com/science/article/pii/S0022369716303900